Journal of ELECTRONIC MATERIALS, Vol. 41, No. 5, 2012
DOI: 10.1007/s11664-011-1881-9

Near-Infrared Absorption in Lattice-Matched AlInN/GaN and Strained AlGaN/GaN Heterostructures Grown by MBE on Low-Defect GaN Substrates

C. EDMUNDS,[1,6] L. TANG,[1] D. LI,[1] M. CERVANTES,[1] G. GARDNER,[2] T. PASKOVA,[3] M.J. MANFRA,[1,2,4,5] and O. MALIS[1]

1.—Department of Physics, Purdue University, West Lafayette, IN 47907, USA. 2.—Birck Nanotechnology Center, West Lafayette, IN 47907, USA. 3.—Kyma Technologies Inc., Raleigh, NC 27617, USA. 4.—School of Materials Engineering, Purdue University, West Lafayette, IN 47907, USA. 5.—School of Electrical and Computer Engineering, Purdue University, West Lafayette, IN 47907, USA. 6.—e-mail: cedmunds@purdue.edu

We have investigated near-infrared absorption and photocurrent in lattice-matched AlInN/GaN and strained AlGaN/GaN heterostructures grown by molecular-beam epitaxy (MBE) on low-defect GaN substrates for infrared device applications. The AlGaN/GaN heterostructures were grown under Ga-rich conditions at 745°C. Material characterization via atomic force microscopy and high-resolution x-ray diffraction indicates that the AlGaN/GaN heterostructures have smooth and well-defined interfaces. A minimum full-width at half-maximum of 92 meV was obtained for the width of the intersubband absorption peak at 675 meV of a 13.7 Å GaN/27.5 Å $Al_{0.47}Ga_{0.53}N$ superlattice. The variation of the intersubband absorption energy across a 1 cm × 1 cm wafer was ±1%. An AlGaN/GaN-based electromodulated absorption device and a quantum well infrared detector were also fabricated. Using electromodulated absorption spectroscopy, the full-width at half-maximum of the absorption peak was reduced by 33% compared with the direct absorption measurement. This demonstrates the suitability of the electromodulated absorption technique for determining the intrinsic width of intersubband transitions. The detector displayed a peak responsivity of 195 μA/W at 614 meV (2.02 μm) without bias. Optimal MBE growth conditions for lattice-matched AlInN on low-defect GaN substrates were also studied as a function of total metal flux and growth temperature. A maximum growth rate of 3.8 nm/min was achieved while maintaining a high level of material quality. Intersubband absorption in AlInN/GaN superlattices was observed at 430 meV with full-width at half-maximum of 142 meV. Theoretical calculations of the intersubband absorption energies were found to be in agreement with the experimental results for both AlGaN/GaN and AlInN/GaN heterostructures.

Key words: Intersubband absorption, near infrared, quantum well infrared photodetector, electromodulation, III-nitride semiconductors, molecular-beam epitaxy

INTRODUCTION

III-nitride semiconductors have several notable material properties that make them promising candidates for infrared light emitters and detectors operating in several technologically relevant spectral regions. The conduction band offset (CBO) of III-nitrides can exceed 1 eV, allowing for operation in the near-infrared range of the spectrum (1.5 μm to 3 μm).[1–6] Moreover, III-nitrides have recently attracted attention due to potential applications in

(Received July 29, 2011; accepted December 20, 2011; published online February 1, 2012)

THz quantum cascade lasers (QCLs).[7–10] GaN has a relatively large longitudinal-optical (LO) phonon energy (~90 meV), which will allow III-nitride-based QCLs to operate in the far-infrared (15 μm to 70 μm), a range that is inaccessible to the well-developed arsenide QCLs. However, the fabrication of III-nitride intersubband (ISB) devices is still challenging due to the high defect density that hinders vertical transport. The high defect density is in large part related to the lattice mismatch between GaN and the commonly used substrates, such as sapphire. In addition to the problems presented by the substrate mismatch, there are also strain-generated dislocations due to the lattice mismatch between the well and barrier materials. Most III-nitride intersubband devices reported in the literature utilize AlGaN/GaN heterostructures for which there is no lattice-matched aluminum composition.[1–4] This material combination is not ideal for the development of complex devices such as QCLs that often require active-region thicknesses on the order of microns for efficient operation.

In this study we demonstrate near-infrared absorption and photocurrent measurements in high-quality lattice-matched AlInN/GaN and strained AlGaN/GaN heterostructures grown by molecular-beam epitaxy (MBE) on low-defect *c*-axis GaN substrates. It has been previously shown that the number of defects in the heterostructures is drastically reduced by the use of thick GaN templates (50 μm to 100 μm) grown by hydride vapor-phase epitaxy (HVPE) on sapphire,[11] and of commercially available free-standing substrates.[12] The free-standing GaN substrates have dislocation densities of the order of 10^6 cm^{-2}, while GaN templates grown on sapphire substrates typically have dislocation densities ~10^8 cm^{-2}. To further mitigate defect generation in thick nitride heterostructures, we also took advantage of the exact lattice matching between GaN and AlInN at around 18% In composition. For both lattice-matched AlInN/GaN and strained AlGaN/GaN heterostructures the MBE growth process on the two types of low-defect substrates was optimized and the material properties were determined with structural techniques and infrared optical and photocurrent spectroscopy.

RESULTS

MBE Growth of AlGaN/GaN and AlInN/GaN Heterostructures

High-quality MBE growth of AlGaN/GaN heterostructures was achieved under Ga-rich conditions at 745°C. Nitrogen was supplied using a radiofrequency plasma source with power of 300 W and flow rate of 0.5 SCCM (SCCM denotes standard cubic centimeters per minute at STP). This resulted in a growth rate of 7.2 nm/min for GaN and 10.5 nm/min for AlGaN with Al composition of around 50%. Silicon doping levels were calibrating using secondary-ion mass spectrometry. The AlGaN/GaN superlattices were characterized using a PANalytical X'Pert-MRD high-resolution x-ray diffractometer (HRXRD) equipped with a four-bounce Ge monochromator. Theoretical simulation of the diffraction pattern using the commercial software package PANalytical X'PERT EPITAXY enabled estimation of the well and barrier thicknesses as well as the Al composition. Figure 1 shows the x-ray diffraction of a 15-repeat 27.5 Å $Al_{0.47}Ga_{0.53}N$/13.7 Å GaN superlattice (sample A, see Table I). The superlattice was grown over a 2000 Å GaN buffer on a free-standing GaN substrate. The quantum wells were continuously doped with Si at a level of 7×10^{19} cm^{-3} and delta doped after the growth of the well at 2×10^{13} cm^{-2}. The narrow superlattice fringes in the diffraction pattern indicate the existence of sharp interfaces (Fig. 1). A surface roughness of 0.65 nm over 4 μm × 4 μm was determined by atomic force microscopy (AFM). All AlGaN/GaN heterostructures are believed to be strained, except the photodetector (sample D), because they show no evidence of cracking. In order to optimize the growth of AlInN heterostructures on the free-standing substrates, we first studied the growth of AlInN films. The growth of AlInN films requires a different approach from that of typical AlGaN MBE growth.[13] While high-quality AlN growth occurs only at high temperature, indium is only incorporated at lower temperatures. Therefore, to achieve sufficient indium composition for lattice-matched AlInN films, we chose a lower growth temperature of 530°C. The growth rate was studied under nitrogen-rich conditions as a function of increasing total metal flux with In/Al flux ratio of ~0.8. The growth rate was found to increase linearly with increasing metal flux. However, the material quality deteriorates significantly at total metal flux of 13.4×10^{-8} Torr. At this flux level,

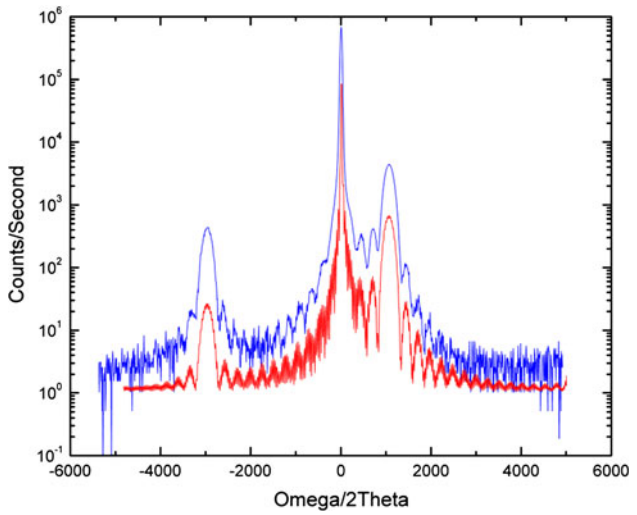

Fig. 1. High-resolution x-ray diffraction (blue curve) and simulation of the scattering pattern (red curve) around the (0002) GaN peak for sample A (Color figure online).

Table I. Structural properties and peak intersubband absorption energies of the heterostructures

Sample	Number of Repeats	Barrier Material	Barrier Thickness (Å)	Well Thickness (Å)	ISB Energy (meV)
Sample A	15	$Al_{0.47}Ga_{0.53}N$	27.5	13.7	675
Sample B	20	$Al_{0.86}In_{0.14}N$	30	30	430
Sample C	6	$Al_{0.55}Ga_{0.45}N$	30	20	487
Sample D	15	$Al_{0.55}Ga_{0.45}N$	31	15	583

root-mean-square (RMS) roughness increased to 4 nm over 2 μm × 2 μm and cracks appeared. Therefore, we have determined that the trend of increasing growth rate while maintaining high material quality ends at 3.8 nm/min, where RMS roughness of 0.8 nm over 4 μm × 4 μm was obtained for a 175 nm $Al_{0.85}In_{0.15}N$ film. High-resolution transmission electron microscopy (HR-TEM) carried out on a cross-section of this film indicates that no threading dislocations were generated in the thick AlInN layer. However, weak stripes along the growth direction were visible under high-angle annular dark-field scanning transmission electron microscopy (HAADF-STEM), suggesting that the alloy composition is laterally inhomogeneous on the scale of a few nanometers. Using the growth parameters discussed above, AlInN/GaN heterostructures of 20 repeats were grown and characterized with HRXRD. In the most uniform sample, the RMS roughness was measured to be 0.65 nm over 4 μm × 4 μm, comparable to the roughness of the free-standing GaN substrates (0.60 nm over 4 μm × 4 μm). Strong superlattice and interference fringes indicate high material quality (Fig. 2). The AlInN/GaN heterostructures were continuously doped with Si in both the well and barrier at 7×10^{19} cm^{-3} and delta doped before growth of the well at 2×10^{13} cm^{-2}.

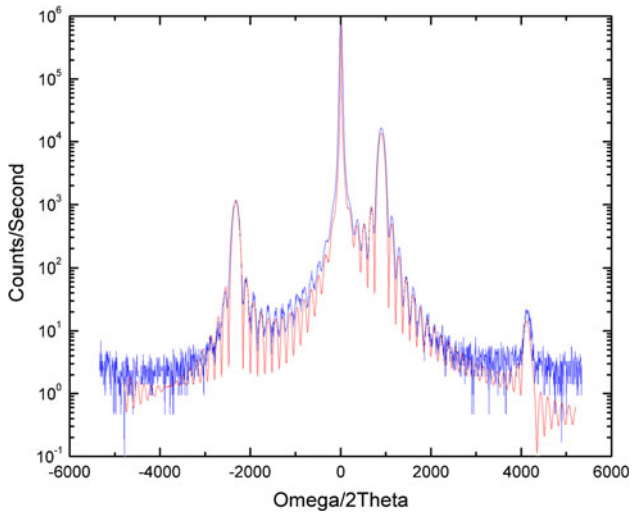

Fig. 2. High-resolution x-ray diffraction (blue curve) and simulation of the scattering pattern (red curve) around the (0002) GaN peak for an InAlN/GaN heterostructure with 20 Å GaN wells and 31.5 Å $Al_{0.85}In_{0.15}N$ barriers (Color figure online).

Direct Absorption in AlGaN/GaN and AlInN/GaN Heterostructures

The infrared properties of the samples were characterized using a Thermo-Nicolet Fourier-transform infrared (FT-IR) spectrometer, a wire-grid polarizer, and a beam condenser. The optical spectra were obtained for both *p*- and *s*-polarizations using the internal white light source and a liquid-nitrogen-cooled InSb detector. The *p*- and *s*-polarized spectra were normalized to reference spectra taken in the absence of any sample. The effect of intersubband absorption was isolated by taking the ratio of the *p*- and *s*-polarized spectra. For the AlGaN/GaN heterostructure (sample A), the intersubband absorption is so strong that it can be measured directly in a single pass through the free-standing wafer. Light was focused into a 3-mm beam at the Brewster's angle. The ratio of the *p*- and *s*-polarized spectra after background subtraction is shown in Fig. 3. The intersubband absorption peak is located at 675 meV (1.84 μm), well within the technologically relevant near-infrared range. The low full-width at half-maximum (FWHM) of 94 meV is attributed to smooth interfaces and well-defined quantum wells. This result is comparable to other recent reports using doped AlN/GaN heterostructures.[4] We also conducted mapping of the intersubband absorption to probe the variation of growth conditions across the 1 cm × 1 cm free-standing GaN wafer (inset of Fig. 3). The variation of the intersubband transition energy was found to be less than ±1%, indicating excellent thickness uniformity across the wafer.

In the case of the AlInN samples, the absorption was too small to measure in single-pass geometry. Therefore, the facets of the sample were polished at 45° in order to fabricate a multipass waveguide. Figure 4 shows an absorption spectrum from an AlInN/GaN superlattice with 30 Å GaN quantum wells and 30 Å $Al_{0.86}In_{0.14}N$ barriers (sample B). The absorption peak is located at 430 meV (2.9 μm). The FWHM of 142 meV is considerably broader than in the AlGaN/GaN heterostructures. This may be attributed to increased quantum well roughness, which is indirectly reflected in the increase of the surface roughness shown by AFM. Surface roughness in sample B was 2.1 nm over 4 μm × 4 μm as opposed to 0.65 nm in sample A, 0.8 nm in bulk

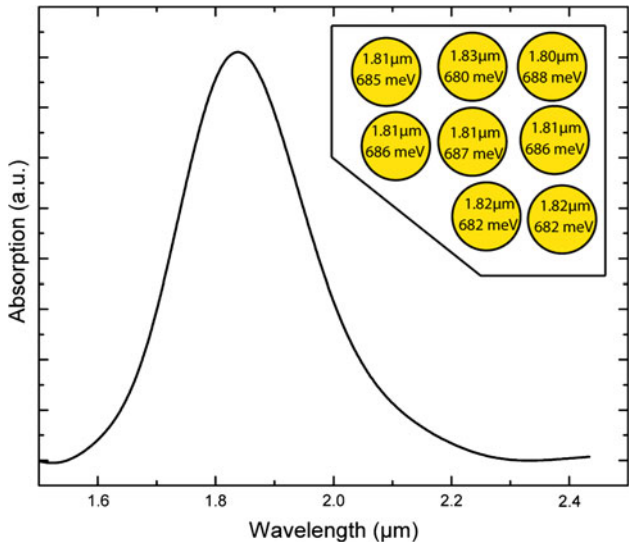

Fig. 3. Ratio of *p*- and *s*-polarized spectra after background subtraction for sample A. The upper right corner shows a map of the intersubband absorption energy across the 1 cm × 1 cm wafer, where each circle indicates the 3 mm diameter of the incident beam.

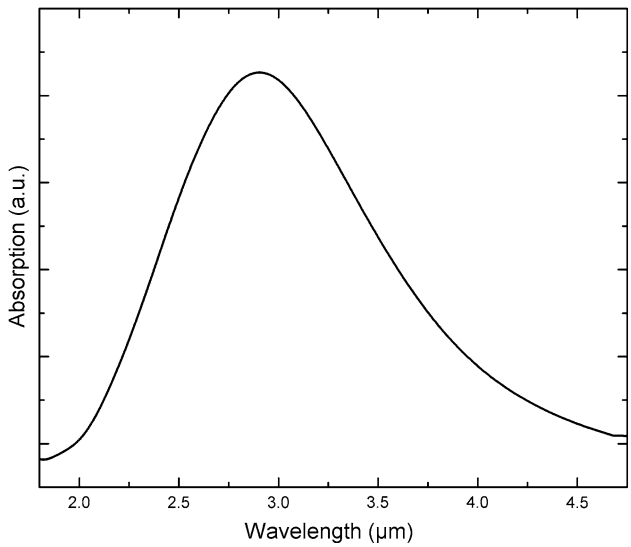

Fig. 4. Ratio of *p*- and *s*-polarized spectra after background subtraction for sample B.

AlInN, or 0.6 nm for the free-standing substrates. Despite this, the ratio of the linewidth and transition energy is similar to the one reported by Nicolay et al.[14] in lattice-matched AlInN/GaN heterostructures grown by metalorganic vapor-phase epitaxy (MOVPE) and is an important indication of material quality. Furthermore, the results in Ref. 14 were obtained by photoinduced absorption. The direct measurement of intersubband absorption in AlInN/GaN heterostructures is an important step towards the realization of AlInN/GaN intersubband devices.

Simulations of the intersubband absorption energies were done using a one-dimensional Schrodinger–Poisson solver.[15] Both piezoelectric and spontaneous polarization fields were considered. The currently accepted values of the relevant material parameters such as the CBO and polarization constants were used.[16] In the case of the AlGaN/GaN heterostructure (sample A), the material parameters from Ref. [16] led to a total polarization field of 3.4 MV/cm in the quantum wells and a CBO of 1.0 meV. The energy of the ground state to first excited state transition was calculated to be 653 meV, which is close to the experimentally measured value of 675 meV. For the AlInN/GaN heterostructure (sample B) a CBO of 1.1 eV was extrapolated from the recent experimental work by Moses et al.,[17] who studied the CBO at various indium compositions. The polarization field in the quantum wells was found to be 3.4 MV/cm. These material parameters resulted in a calculated energy of 401 meV, in agreement with the experimental value.

Electromodulated Absorption in AlGaN/GaN Heterostructures

To investigate the intrinsic linewidth of the intersubband transitions an AlGaN/GaN intersubband electromodulator was fabricated.[18] Electromodulated absorption spectroscopy is a more sensitive technique than direct absorption, allowing measurements at lower doping levels or from a smaller number of wells. Therefore, to minimize the effect of well-to-well thickness variation on broadening and investigate the intrinsic linewidth of the intersubband transitions in a single well, we fabricated an intersubband electromodulated absorption device containing a small number of quantum wells. The device consisted of six repeats of nominally 20 Å GaN quantum wells and 30 Å $Al_{0.55}Ga_{0.45}N$, sandwiched between a 40 Å $Al_{0.55}Ga_{0.45}N$ cap and a 2000 Å GaN buffer (sample C, Fig. 5). Mesas (1 mm × 0.5 mm) were defined using standard photolithography techniques and chlorine plasma dry-etching. The top of the mesas was covered with a 3000 Å layer of Si_3N_4, and Ti/Al/Ni/Au contacts (25 nm/125 nm/45 nm/55 nm) were deposited using electron-beam evaporation. The sample was then polished into a multipass waveguide and characterized using FT-IR spectroscopy. The ratio of the *p*- and *s*-polarized spectra after background subtraction displays an intersubband absorption peak at 487 meV with FWHM of 208 meV (Fig. 5). This rather large FWHM of the intersubband absorption peak is attributed to the relatively high RMS roughness of 3.6 nm over 4 μm × 4 μm of this particular sample.

To carry out electromodulated absorption experiments, a voltage of 2 V was applied across the device with the positive terminal over the mesa. The voltage was pulsed at 1 kHz, and the signal on the InSb detector was analyzed using a lock-in amplifier for both *p*- and *s*-polarized light. The intersubband absorption peak was measured at 478 meV with FWHM of 139 meV (Fig. 6). The

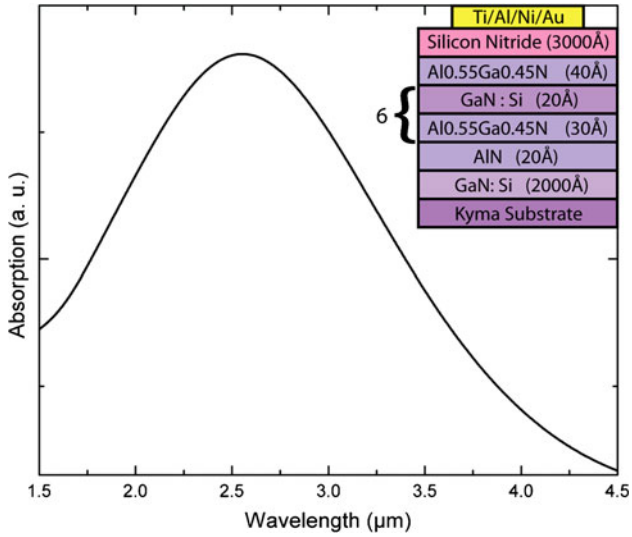

Fig. 5. Ratio of *p*- and *s*-polarized spectra after background subtraction for sample C. The device structure is shown in the upper right corner.

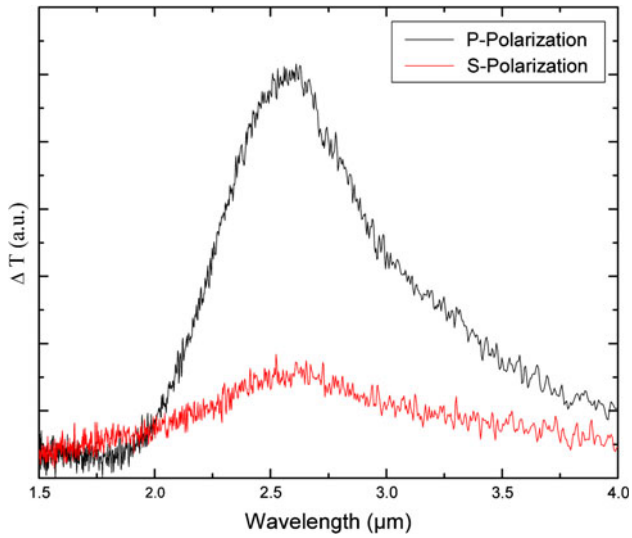

Fig. 6. *p*- (black) and *s*-polarized (red) electromodulated absorption for sample C (Color figure online).

presence of a relatively weak signal in the *s*-polarization may be due to light depolarization through scattering. Although the intersubband transition energy was similar for the two absorption experiments, the FWHM decreased by 33% in the electromodulated absorption measurement. This result can be understood by simulating the charge distribution in the heterostructure under bias. As seen in Fig. 7, only the electron density in the well closest to the surface undergoes an appreciable change in the presence of an applied bias. Therefore, the electromodulated signal is likely dominated by the intersubband absorption in this topmost well. Moreover, the peak FWHM is a direct measurement of broadening due to interface roughness in this single well.

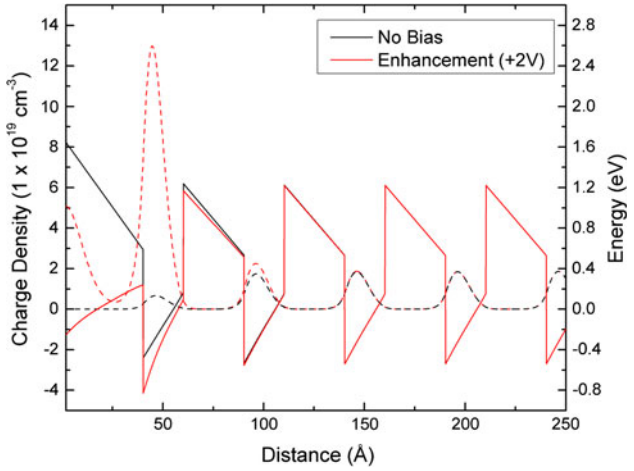

Fig. 7. Theoretical simulation of the charge density (dashed line) and band structure (solid line) in the first four wells of sample C at no bias (black) and +2 V (red) (Color figure online).

Absorption and Photocurrent Characterization of an AlGaN/GaN Quantum Well Infrared Photodetector

To test vertical transport on low-defect GaN substrates we also fabricated and characterized AlGaN/GaN quantum well infrared detectors (QWIPs). The QWIP structure consisted nominally of 15 repeats of 15 Å GaN quantum wells and 31 Å $Al_{0.55}Ga_{0.45}N$ barriers sandwiched between 561 Å GaN bottom and 72 Å GaN top highly doped contact layers (sample D, Fig. 8). Before device fabrication, direct absorption was measured in single-pass geometry at the Brewster's angle and indicated a peak at 583 meV with FWHM of 110 meV. The details of the device processing are identical to those for the electromodulated device, except for the ohmic contact to the top of the mesa. The photocurrent measurement was done at room temperature under zero bias using a lock-in amplifier, a white light source, and an optical chopper. To allow for effective optical coupling, the sample was polished into a 45° multipass waveguide such that the incoming radiation was incident on the mesa during the first pass. The unpolarized photocurrent measurement consists of a broad background and a narrower peak (Fig. 8). The broad background, which is not polarization sensitive, may be due to absorption in the contact regions. To isolate the intersubband photocurrent, the *p*- and *s*-polarization photocurrent spectra were normalized to polarized photocurrent spectra of a thermal detector with a flat response. These spectra were then normalized to each other to eliminate the polarization-independent component (Fig. 9). The peak responsivity was measured to be 195 μA/W at 614 meV (2.02 μm). The blueshift of the photocurrent peak with respect to the direct absorption measurement has been observed previously in the literature and is expected since the photocurrent spectrum is the product of the intersubband line profile and the

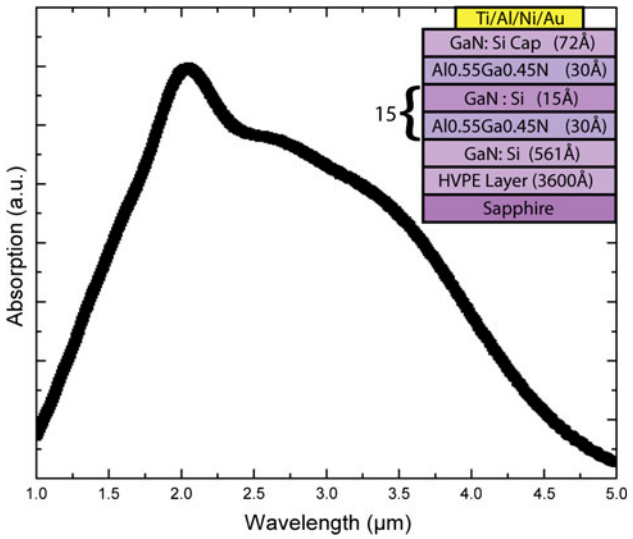

Fig. 8. Unpolarized photocurrent signal for sample D. The device structure can be seen in the upper right corner.

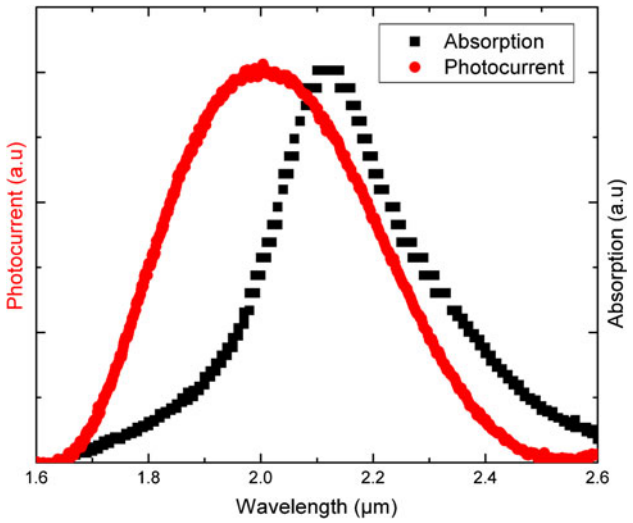

Fig. 9. Ratio of *p*- and *s*-polarized intersubband absorption spectra (black) and photocurrent signals (red) after background subtraction for sample D.

electron tunneling probability, which increases with energy.[19] The FWHM of the polarization normalized photocurrent was 161 meV.

CONCLUSIONS

We have completed an in-depth study of the optimal MBE growth conditions of AlGaN/GaN and AlInN/GaN heterostructures on low-defect GaN substrates for infrared device applications. X-ray diffraction and AFM studies indicate smooth surfaces and sharp interfaces between layers. The uniformity of quantum wells is corroborated by the low FWHMs of the intersubband absorption peaks and the consistency of the intersubband absorption energy across a 1 cm × 1 cm wafer. The intersubband absorption energies were found to be well reproduced with the currently accepted material parameters. In addition, an intersubband electromodulated absorption device and a QWIP were fabricated. Using the electromodulation absorption technique, we observed a 33% reduction of the FWHM relative to the direct absorption measurement. This demonstrates the suitability of this technique for minimizing extrinsic sources of broadening and for determining the width of the intersubband transitions, an important quantity in the calculation of the gain for nitride-based QCLs. Finally, the demonstration of the AlGaN/GaN QWIP on low-defect substrates represents an important step towards more complex vertical transport devices.

ACKNOWLEDGEMENT

The authors acknowledge support from the NSF Award ECCS-1001431 and from the Defense Advanced Research Project Agency (DARPA) under Contract No. D11PC20027. We thank Dr. R.J. Molnar from MIT Lincoln Laboratories for providing the GaN templates grown by HVPE on sapphire and R. Colby for TEM and HAADF-STEM images.

REFERENCES

1. C. Gmachl, H.M. Ng, and A.Y. Cho, *Appl. Phys. Lett.* 77, 334 (2000).
2. C. Gmachl, H.M. Ng, and A.Y. Cho, *Appl. Phys. Lett.* 79, 1590 (2001).
3. C. Gmachl and H.M. Ng, *Electron. Lett.* 39, 567 (2003).
4. M. Tchernycheva, L. Nevou, L. Vivien, F.H. Julien, P.K. Kandaswamy, E. Monroy, and A. Vardi, *Phys. Status Solidi B* 247, 1622 (2010).
5. O. Malis, C. Edmunds, M.J. Manfra, and D.L. Sivco, *Appl. Phys. Lett.* 94, 161111 (2009).
6. O. Malis, C. Edmunds, D. Li, and M.J. Manfra, *18th Biennial University/Government/Industry Micro-Nano Symposium "Intersubband transitions in lattice-matched AlInN/GaN Heterostructures"* (2010).
7. G. Sun, *J. Lumin.* 119–120, 528 (2006).
8. H. Machhadani, Y. Kotsar, S. Sakr, M. Tchernycheva, R. Colombelli, J. Mangeney, E. Bellet-Amalric, E. Sarigiannidou, E. Monroy, and F.H. Julien, *Appl. Phys. Lett.* 97, 191101 (2010).
9. E. Bellotti, K. Driscoll, T.D. Moustakas, and R. Paiella, *Appl. Phys. Lett.* 92, 101112 (2008).
10. E. Bellotti, K. Driscoll, T.D. Moustakas, and R. Paiella, *J. Appl. Phys.* 105, 113103 (2009).
11. R.J. Molnar, W. Götz, L.T. Romano, and N.M. Johnson, *J. Cryst. Growth* 178, 147 (1997).
12. T. Paskova, D.A. Hanser, and K.R. Evans, *Proc. IEEE* 89, 1324 (2010).
13. S. Schmult, T. Siegrist, A.M. Sergent, M.J. Manfra, and R.J. Molnar, *Appl. Phys. Lett.* 90, 021922 (2007).
14. S. Nicolay, J.-F. Carlin, E. Feltin, R. Butté, M. Mosca, N. Grandjean, M. Ilegems, M. Tchernycheva, L. Nevou, and F.H. Julien, *Appl. Phys. Lett.* 87, 111106 (2005).
15. G. Snider, *D Poisson Program*. University of Notre Dame. http://www.nd.edu/~demand.
16. J. Wu, *J. Appl. Phys.* 106, 011101 (2009).
17. P.G. Moses, M. Miao, Q. Yan, and C.G. Van de Walle, *J. Chem. Phys.* 134, 084703 (2011).
18. E. Baumann, F.R. Giorgetta, D. Hofstetter, S. Leconte, F. Guillot, E. Bellet-Amalric, and E. Monroy, *Appl. Phys. Lett.* 89, 101 (2006).
19. D. Hofstetter, Sven-Silvius Schad, H. Wu, W.J. Schaff, and L.F. Eastma, *Appl. Phys. Lett.* 82, 572 (2003).